King's Research Portal

Link to publication record in King's Research Portal

Citation for published version (APA):
Hamdi, M., Abdel-Bar, H. M., Elmowafy, E., Al-Jamal, K. T., & Awad, G. A. S. (2020). An integrated vitamin E-coated polymer hybrid nanoplatform: A lucrative option for an enhanced in vitro macrophage retention for an anti-hepatitis B therapeutic prospect. *PLoS ONE, 15*(1), e0227231. Article e0227231. https://doi.org/10.1371/journal.pone.0227231
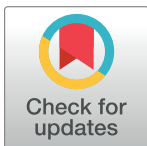
An integrated vitamin E-coated polymer hybrid nanoplatform: A lucrative option for an enhanced *in vitro* macrophage retention for an anti-hepatitis B therapeutic prospect

Mohamed Hamdi[1], Hend Mohamed Abdel-Bar[1]*, Enas Elmowafy[2], Khuloud T. Al-Jamal[3], Gehanne A. S. Awad[2]

1 Department of Pharmaceutics, Faculty of Pharmacy, University of Sadat City, Sadat City, Egypt,
2 Department of Pharmaceutics and Industrial Pharmacy, Faculty of Pharmacy, Ain Shams University, Sadat City, Egypt, **3** Institute of Pharmaceutical Science, Faculty of Life Sciences & Medicine, King's College London, England, United Kingdom

* hend.abdelbar@fop.usc.edu.eg

Abstract

A platform capable of specifically delivering an antiviral drug to the liver infected with hepatitis B is a major concern in hepatology. Vaccination has had a major effect on decreasing the emerging numbers of new cases of infection. However, the total elimination of the hepatitis B virus from the body requires prolonged therapy. In this work, we aimed to target the liver macrophages with lipid polymer hybrid nanoparticles (LPH), combining the merit of polymeric nanoparticles and lipid vesicles. The hydrophilic antiviral drug, entecavir (E), loaded LPH nanoparticles were optimized and physicochemically characterized. A modulated lipidic corona, as well as, an additional coat with vitamin E were used to extend the drug release enhance the macrophage uptake. The selected vitamin E coated LPH nanoparticles enriched with lecithin-glyceryl monostearate lipid shell exhibited high entrapment for E (80.47%), a size $\leq$ 200 nm for liver passive targeting, extended release over one week, proven serum stability, retained stability after refrigeration storage for 6 months. Upon macrophage uptake *in vitro* assessment, the presented formulation displayed promising traits, enhancing the cellular retention in J774 macrophages cells. *In vivo* and antiviral activity futuristic studies would help in the potential application of the ELPH in hepatitis B control.

1. Introduction

Lately an increased alertness about the role of hepatic macrophages in viral hepatitis has been recognized [1, 2]. Being members of the reticuloendothelial system, they have been acknowledged as key participants in the prevention of the disease progression [2]. Delivery strategies using nanotherapeutics to target the macrophages had been well specified [3]. The nanocarriers should possess a defined size, with a targeted engineered modified surface to facilitate both passive and active (cellular targeting) liver targeting [4].

Hepatitis B virus (HBV) infection accounts for increased deaths worldwide, due to the risk of cirrhosis, hepatocellular cancer, portal hypertension and liver failure [5]. To date, the antiviral therapies, have failed to realize complete removal of the virus from the body and treatment prolonged duration, without the possible emergence of drug resistance [6, 7]. Due to its high lethality, researchers advanced that in the future, good therapy of HBV should be a composite treatment build up from nucleot(s)ide analogs, immunostimulants and possibly curative vaccines.

Among the antiviral nucleot(s)ide analogues, entecavir (E), has been highly recommended due to various merits: (i) potency, (ii) low resistance, and (iii) low systemic toxicity [8–10]. In a very recent multicenter cohort study conducted by Chinese researchers, E monotherapy offered evidence of lowered virological breakthrough and heightened HBV-DNA suppression compared to combination therapy of antiviral agents; lamivudine and adefovir [9]. Zoutendijk and coworkers suggested E monotherapy for 48 weeks [11]. However, the oral administration of E is associated with poor patient compliance and adverse reactions, resulting from intake of E on empty stomach, necessitating the fabrication of sustained release formulation [6]. In this context, long-acting parenteral formulations of E have been well-investigated by various research groups, including liquid crystals [12], lipidic prodrug [13], albumin nanoparticles [8] and PLGA microspheres [6].

Highly optimized carriers with sub-cellular targeting moieties have been opted to enhance hepatic (Kupffer cells and hepatocytes) targeting efficiency for competent antiviral delivery [5]. Fabrication of polymeric nanoparticles and lipid nanocarriers is considered as the most noticeable tool to fulfill such purpose. Polymeric nanoparticles have been employed to provide good hydrophobic drug loading, biodegradability, structural integrity and stability characteristics [14, 15]. On the other hand, the use of lipid nanocarriers such as liposomes is well-consolidated, due to their good biocompatibility as well as the ease of modification by different targeting moieties [16], Besides, up till now, they are the only nanocarriers being approved in clinical applications and scaled-up for industrial production [17]. However, both nanocarriers, when utilized separately, have some limitations due to poor loading of hydrophilic bioactive compounds and uncontrolled drug release from polymeric nanoparticles and drug leakage and instability during storage from lipid nanocarriers [18, 19].

Hence, lipid-polymer hybrid nanoparticles (LPH) was designed, combining the advantages of both polymer- and lipid-based nanoparticles. LPH are archetype of nanocarriers composed of an internal polymeric core enclosed by an outer lipid bioactive shell composed of one or more layers or components [20, 21]. By virtue of their unique structure, LPH have versatile competence to encapsulate different types of payloads such as hydrophilic, hydrophobic drugs or nucleic acids, highlighting promising *in vivo* therapeutic outcomes [22–25]. The concomitance of both polymer and lipid imparts the LPH structural integrity, serum stability, sustained drug release (from the polymer core) and high biocompatibility (from the lipid shell) [21]. Finally, rapid opsonization induced by the lipidic shell resulting in rapid uptake of the particles by the mononuclear phagocyte system (MPS) in the liver and spleen has been previously proven [26, 27].

Different polymers and lipids have been exploited for the fabrication of LPH. PLGA, a synthetic polyester, approved by US FDA and European Medicine Agency for human use has been extensively investigated in the fabrication of LPH [28]. Lecithin (LEC) is a type of phospholipids which are vital components of the cell membrane to conserve membrane fluidity [29]. Generally, phospholipids play a crucial role in solubilization, sustainment of drug release, improvement of therapeutic efficacy and biocompatibility [30, 31].

In light, the aim of this study is to formulate and evaluate a new long-acting macrophage-directed platform for the antiviral agent E. This work provides the first utilization of LPH in E

(ELPH) parenteral delivery. The optimized formulae, obtained from Box-Behnken (BBD) statistical design, were subjected to different modulations to prolong the drug release to the maximum. Firstly, lecithin (LEC) lipid shell was admixed with other lipids such as cholesterol (CH) or glyceryl monostearate (GMS) and secondly the NPs were further coated with vitamin E. Both CH and GMS have been reported to control drug release from different carriers [32, 33].

CH is well-reputed neutral lipid commonly used in liposomes, heightening the packing of phospholipid molecules, rigidity and stabilization of liposomes [34]. GMS is a single-chained biocompatible self-assembly amphiphilic monoglyceryl ester, showing significant applications in drug delivery as self-nanoemulsifying drug delivery systems, solid lipid nanoparticles, polymer lipid nanoparticles [35–37]

Vitamin E, is a lipid soluble vitamin with antioxidant [38] and immunomodulatory activities [39]. It has been reported to improve the phagocytic potential of macrophage in broilers [40]. Moreover, it has several transport pathways from serum to liver by different vitamin E–binding proteins as α-tocopherol-associated proteins (SEC14L2, SEC14L3, and SEC14L4) and the albumin-related protein, afamin[41, 42].

It is worth mentioning that this investigation assesses for the first time macrophage targeting of vitamin E coated E loaded nanopharmaceuticals, as an indicator of the efficient hepatic therapeutic system, an issue that has not been attempted yet in previously reported E carriers. In this regard, confocal laser scanning microscopy (CLSM) and flow cytometry was performed to evaluate the qualitative and quantitative macrophage retention of ELPH respectively.

2. Materials and methods

2.1. Materials

Entecavir (E): kindly provided by Mash Premiere for Pharmaceutical Industry, Egypt. Glyceryl monostearate (GMS): purchased from Carl Roth GmbH, Germany. 50/50 DL-lactide/glycolide conjugate, acid terminated (PLGA, with an inherent viscosity midpoint of 0.2 dl/g): kindly supplied from Purac Biomaterials. Lecithin (LEC) soybean (3-*sn*-Phosphatidylcholine ≥99% (TLC) lyophilized powder), cholesterol (CH), vitamin E (α-Tocopherol ≥95.5%), acetonitrile (HPLC grade), ethanol absolute, dimethylformamide (DMF), dimethylsulphoxide (DMSO), 4′,6-Diamidino-2-phenylindole (DAPI), RPMI and fetal bovine serum (FBS): purchased from Sigma–Aldrich Company, UK. Mannitol: purchased from BDH Chemicals Ltd, Poole, UK. Potassium dihydrogen orthophosphate, sodium hydroxide, sodium chloride, potassium chloride, sodium dibasic hydrogen orthophosphate, hydrochloric acid and Tween 80 (polysorbate 80): obtained from Fluka Chemika-BioChemika, Switzerland. Triton™ X-100 and 1,1'-Dioctadecyl-3,3,3',3'-Tetramethylindocarbocyanine Perchlorate (DiI): purchased from Fisher Scientific, UK. Vectashield® mounting media was from Vector Labs (UK).

2.2 Methods

2.2.1. Determination of entecavir solubility in different lipids. The solubility of entecavir (E) in different single lipids or different mixtures of LEC with CH or GMS was determined as described in supplementary information [43, 44].

2.2.2. Preparation of E LPH. Different formulations ELPH were prepared using modified single-step nanoprecipitation self-assembly method as described elsewhere [14]. Briefly, different amounts of PLGA and E were dissolved in DMF forming the organic phase. According to the output needed from the study, the aqueous phase containing different weights of LEC with or without CH or GMS and Tween 80 (1% w/v) were dissolved in 4%v/v hydroalcoholic solution and heated to 70˚C for 15 min. The amounts and concentrations of polymers/lipids in different ELPH formulations are listed in Table 1. Slow dripping of the organic phase into the

Table 1. Levels of critical process parameters for the preparation of ELPH using the BBD.

Critical process parameters (Coded independent variables)[a]	Levels		
	Low (-1)	Medium (0)	High (1)
A: PLGA (mg)	5	10	15
B: LEC (mg)	1	2	3
C:Drug (mg)	5	10	15
D:Stirring speed (rpm)	500	750	1000

[a] The quality attributes and quality target product profiles was PS ($<$ 200 nm) and maximum Entrapment efficiency (EE %).

https://doi.org/10.1371/journal.pone.0227231.t001

aqueous phase was done while stirring at room temperature for 2 h. The ratio of organic to aqueous phase was kept at 1:9 v/v. The resultant LPH dispersions were centrifuged at 12000 rpm for 30 min at 4˚C and the harvested pellets were re-suspended in PBS (pH 7.4) for further analysis. The optimized ELPH was incubated with vitamin E (1 mL for 2h) to produce EELPH. After soaking, the dispersions was re-centrifuged under the same conditions to remove excess vitamin E. For estimations of entrapment efficiency (EE %) and loading capacity (LC), a fixed volume was removed before centrifugation as a total drug reference. DiI-labelled ELPH and EELPH were prepared by dissolving the dye into the lipid phase at 1% w/w. Freeze-dried ELPH and EELPH were obtained after 48h lyophilization to obtain a free-flowing powder, when required.

2.2.3. Experimental design and construction of Box-Behnken (BBD) design. Optimization of ELPH was done using BBD (Design-Expert 9.0.5.2, State-Ease Inc., USA) to construct matrix and explore both the response surfaces and the statistical models [45]. The selected critical process parameters (CPPs) i.e. the independent variables were PLGA, LEC, E amounts and stirring speed which respectively labelled as A, B, C and D. Each variable was tested at three levels; low (-1), medium (0) and high (+1). The particle size (PS) (*Y1*) and entrapment efficiency (EE %) (*Y2*) were the critical quality attributes (CQAs). The ELPH were designed to deliver quality target product profile (QTPP) of PS less than 200 nm and maximum EE%. The defined CPPs and CQAs, as well as the desired QTPP, are listed in Table 1.

The design matrix generated by the software consisted of 29 different runs (Table 2). ANOVA was used for the statistical validation of the polynomial equations generated by Design Expert software. All the responses observed were simultaneously fitted to linear; two-factor interactions (2FI) and quadratic models. The three-dimensional (3-D) response surface plots were constructed by the software and the polynomial equations were authenticated.

Based on the highest desirability, the design space was created to define the optimum CPPs [46]. Three optimum checkpoints were picked for validation of the chosen domain and equations. The experimental values of the responses were quantitatively compared with that of the predicted values and prediction error (%) were calculated.

2.2.4. Determination of particle size, size distribution and zeta potential (ξ). The PS (z-average) and size distribution expressed as polydispersity index (PDI) of the prepared ELPH, as well as ξ of the optimized ones, were estimated by dynamic light scattering technique (DLS) with a Nanosizer ZS Series (Malvern Instruments, UK).

2.2.5. Entrapment efficiency and loading capacity. The entrapment efficiency (EE %) was determined directly by measuring the amount of E entrapped inside the LPH. Accordingly, a specified volume of the prepared dispersions (5 mL) was centrifuged at 12000 rpm for 30 min at 4˚C and the collected pellets were dissolved into DMF (10 mL). The amount of encapsulated drug was quantified using a previously validated HPLC method (Agilent 1100, Germany,

Table 2. Experimental design matrix of the CPPS and the related CQAs.

Run	Critical process parameters (CPPs)				Critical quality attributes (CQAs)	
	A PLGA (mg)	B LEC (mg)	C Drug (mg)	D Stirring speed (rpm)	Y1 PS (nm)[a,c]	Y2 EE (%)[b,c]
1	10	2	10	750	150±2	63.21±2
2	15	2	15	750	215±2	77.63±3
3	10	2	15	500	310±3	72.05±1
4	10	3	10	1000	165±3	74.89±3
5	10	2	10	750	160±2	68.09±4
6	10	2	10	750	161±3	69.81±3
7	10	1	10	1000	137±2	76.61±3
8	10	2	10	750	159±2	68.39±4
9	5	2	5	750	134±2	38.25±3
10	15	2	10	500	285±2	59.61±3
11	15	2	5	750	157±4	38.91±3
12	10	3	15	750	189±2	76.84±2
13	10	1	15	750	196±2	78.59±3
14	5	2	15	750	137±4	68.09±4
15	15	3	10	750	194±2	60.16±5
16	10	2	15	1000	190±3	76.51±3
17	5	2	10	500	269±4	55.87±3
18	10	2	5	1000	125±3	46.86±3
19	5	3	10	750	137±4	76.6±3
20	5	1	10	750	128±3	47.09±2
21	5	2	10	1000	138±4	64.41±3
22	15	2	10	1000	169±2	68.54±3
23	15	1	10	750	139±3	75.74±2
24	10	3	10	500	295±2	63.86±4
25	10	2	5	500	266±3	34.09±2
26	10	3	5	750	188±3	51.09±3
27	10	1	10	500	275±3	60.44±1
28	10	2	10	750	180±3	76.59±2
29	10	1	5	750	135±4	40.98±5

[a] PS was measured by DLS.

[b] Calculated as percentage of initial E added, determined directly by HPLC.

[c] Expressed as mean ± SD (n = 3).

https://doi.org/10.1371/journal.pone.0227231.t002

equipped with G 1311A quaternary pump and UV detector (VWD-G1314 A). A reverse phase C18 column (Thermo[®] BDS, 250X4.6 mm, 5μ) was used at 25°C. The wavelength of the UV detector was set at 254 nm. The flow rate of the mobile phase, composed of acetonitrile and 10 mM phosphate buffer pH 3.5 at a ratio of (80:20), was adjusted at 1 mL/min.

The EE % and LC % were calculated according to the following equations [24]:

$$EE\% = \frac{amount\ of\ entecavir\ inside\ the\ pelletes}{Total\ amount\ of\ entecavir\ added} * 100 \tag{1}$$

$$LC\% = \frac{mass\ of\ entecavir\ inside\ the\ pelletes}{Total\ mass\ of\ entecavir\ LPH\ NPs} * 100 \tag{2}$$

2.2.6. *In vitro* drug release study. Aliquots of ELPH or EELPH (equivalent to 5mg E) was placed in the presoaked dialysis membrane (cut off: 10,000 Da), diluted with 1mL of PBS (pH 7.4) and mixed with fresh rat serum (FRS) at 50% v/v final concentration [47]. The dialysis membrane method with slight modifications was used [48]. The tightly closed membranes were put in containers filled with 50 mL PBS (pH 7.4) in a thermostatically controlled shaking water bath at 250 strokes/min ±0.1 at 37±0.5˚C. At predetermined time intervals, an aliquot of 0.5 mL was withdrawn and replaced. The samples were analyzed using the validated HPLC method and the percentage of E released was calculated.

The release profiles were compared by applying the similarity factor (f_2). Two dissolution profiles were considered similar when the f_2 value is $\geq$50 [48].

2.2.7. Morphological studies. *2.2.7.1. Transmission electron microscope (TEM).* EELPH was visualized using transmission electron microscope (TEM, Jeol, JEM-1230, Japan). A drop of the optimized EELPH dispersion was deposited on a copper 300-mesh grid, coated with carbon and allowed to stand for 10min after which, any excess fluid was absorbed by a filter paper. Before the examination, one drop of 1% phosphotungstic acid was applied and allowed to dry for 5min.

2.2.7.2. Atomic force microscope. The 3-D surface profile and topographical image for EELPH were visualized by atomic force microscope (AFM, Wet-SPM 9600, Scanning probe microscope, Shimadzu, Japan.) under normal atmospheric conditions. One drop of the optimized EELPH dispersion was placed on a silicon wafer and allowed for air drying. The measurements were performed using high-resonant-frequency pyramidal cantilevers with silicon probe. The cantilever had a nominal force constant of 0.35–6.06 N/m with a scan speed of 2Hz. The AFM images were analyzed using non-contact mode software [49].

2.2.8. *In vitro* serum stability assay. The *in vitro* stability of EELPH was assessed by recording the PS, PDI and ξ after incubation with 10% and 50% v/v fetal bovine serum (FBS) for 4, 24 and 48 h at 37± 0.5˚C [50].

2.2.9. *In vitro* hemolytic assay. Haemolytic activity of the optimized EELPH was assessed using fresh male albino rat's red blood cells (RBCs). All animal experiments were conducted in agreement with the project license (PBE6EB195) granted by the UK Home Office and in accordance with the U.K. Animals (Scientific Procedures) Act, 1986 and associated guidelines, EU Directive 2010/63/EU for animal experiments. Briefly, blood was withdrawn on heparinized tube from male albino rat (aged 2–3 months, 200g ±10%) tail vein (1 mL from each animal). The blood was centrifuged at 4000 rpm for 10 min to collect the RBCs. The collected RBCs were incubated with different quantities of EELPH and incubated for 2 h at 37˚C. The samples were then centrifuged at 4000 rpm for 5 min at 4 ˚C. The absorbance of each supernatant was determined at 545 nm. The RBCs were incubated with 0.5 w/v% Triton X-100 and PBS (pH 7.4) as positive and negative controls, respectively [51, 52]. Percentage (%) hemolysis was calculated using the following equation:

$$\% \ Hemolysis = \frac{absorbance \ sample - absorbance \ negative \ control}{absorbance \ positive \ control - absorbance \ negative \ control} * 100 \qquad (3)$$

2.2.10. Shelf life stability study. The optimized EELPH were kept at 4˚C for 6 months. PS, ξ, as well as EE% were evaluated after 1, 3 and 6 months as previously described.

2.2.11. *In vitro* cellular uptake study of DiI-labelled ELPH. *2.2.11.1. In vitro MTT cytotoxicity assay.* J774 macrophage cells (catalogue number ATCC® TIB-67™) were purchased from ATCC, UK. Cells were deprived from reticulum cell sarcoma of BALB/cN mice. J774 macrophage cells were seeded in 96-well plate at a density of 10 K/ well in RPMI media and

incubated overnight before being treated with the optimized ELPH or EELPH at serial drug concentrations ranging from 0.01–100 μM. Untreated cells or cells treated with the same concentration range of sodium lauryl sulfate were used as negative and positive control respectively. The *in vitro* cytotoxicity was assessed by MTT assay after 48 h of incubation, media was aspirated and cells were incubated with 120 μL of MTT solution at 37˚C and 5% CO_2. After 4 h, the formed formazan crystals were dissolved in 200 μL of DMSO and the plate read at 570 nm using FLUO star OPTIMA plate reader (BMG Labtech) [53]. The results were expressed as the percentage cell survival and calculated using the following equation:

$$\% \text{ Cell survival} = \frac{\text{A570 nm of treated cells}}{\text{A570 nm of untreated control cells}} * 100 \tag{4}$$

2.2.11.2 Determination of cellular uptake by confocal laser scanning microscope. J774 macrophage cells were seeded onto sterile glass coverslips in 24-well plate at density 50 K cells/ well in RPMI media overnight. After incubation with 50 nM of the optimized DiI-labelled EELPH for 4 and 24 h, the cells were washed by PBS (pH 7.4) and fixed with 200 μL of 4% PFA for 15 min at room temperature. Subsequently, nucleus was counterstained with DAPI and the coverslips were mounted on glass slides by VectaShield™ mounting media. Cells were visualized by confocal laser scanning microscope (CLSM) (Carl Zeiss Microscopy GmbH, Germany) [54].

2.2.11.3 Determination of cellular uptake by flow cytometry. The cellular uptake of DiI-labelled ELPH and EELPH was quantified using flow cytometry (BD FACS Calibur™ flow cytometer, BD Biosciences). An overnight seeded J774 macrophage cells in 24-well plate at density 50 K cells /well were incubated with two different concentrations of the labelled optimized ELPH or EELPH (25 and 50 nM) for 4 and 24 h. Consequently, cells were washed twice with PBS, trypsinized and centrifuged at 1750 rom for 3 min at 4 ˚C. The collected cells were re-suspended into 200 μL of PBS. The uptake study was conducted at 10 K gated cells by quantifying the fluorescence using FL-2 detector and the obtained data was analysed using FlowJo software [55].

2.2.12. Statistical analysis. Three replicates were done for each experiment and the recorded results were the mean ± SD. For comparing two variables student t-test was applied. For comparing different parameters between groups one-way analysis of variance (ANOVA) was applied followed by Tukey HSD test. All the analyses were performed using SPSS 18 (Chicago, USA) and differences were considered significant at probability (*p*) value <0.05.

3. Results and discussion

Designing nanocarriers capable of entrapping hydrophilic drugs in matrices with a delayed degradation, high encapsulating abilities and protected by a stabilizing coat to evade the immune system has attracted various researches in the last decade giving birth to the new progeny of LPH [56]. The molecular lipid barricade has to be optimized for adjusted size and noticeable prolonged release. In this context we aimed to prepare ELPH with high drug EE% and PS suitable for liver targeting of E, adopting a three steps study: 1) an optimization study to achieve the QTPP required for ELPH [57]; 2) a release experiment for the suggested ELPH by the model and finally 3) the effect of vitamin E coating on the optimized LPH physicochemical characteristics.

3.1. Optimization of ELPH using BBD

Generally, the physicochemical properties of nanocarriers affect their intracellular internalization and their subsequent therapeutic applications [58]. In this context, response surface

methodology, using BBD, was constructed to ascertain the effect and interactions of different CPPs on PS (Y1) and EE% (Y2) (Table 2). According to the highest R^2 and the lowest PRESS values, quadratic model was selected as the best fit statistical model for both PS and EE% responses (S1 and S2 Tables).

3.1.1. Effect of different CPPS on Y1 and Y2.   Table 2 shows that the fabricated ELPH had PS ranging between 125–310 nm, while drug EE % varied between 34.09 to 78.59%. All formulae showed a PDI less than 0.25 with a unimodal distribution. The effects of various significant CPPs on PS and EE% were described according to the following equations after omitting the non-significant terms:

$$Y1 = +162 + 18A + 13.17B + 19.33C - 64.67D + 13.75AC - 15.00BC + 56.46D^2 \quad (5)$$

$$Y2 = +69.22 + 2.52A + 2.00B + 16.63C + 5.16D - 11.27AB - 5.07A^2 - 8.94C^2 \quad (6)$$

ANOVA (S3 and S4 Tables) of the data reveals the regression coefficients of all assessed CPPs have p-values <0.05 indicating their significant effect.

According to Eq (5) and Fig 1, it is clear that ELPH PS was positively correlated with ***PLGA (A), lipid (B), drug amounts (C) and AC interaction*** with higher coefficients of ***A and C***. The higher organic phase component amounts, the polymer and the drug, would increase the viscosity of this phase thus decreasing its evaporation rate producing larger PS [59]. Moreover, this thick solution would hinder the breakdown of the droplets into smaller particles, opposing the shear force impact of stirring [60]. Similar findings were previously reported [14, 61, 62]. The positive interaction between ***A and C*** indicates an enhanced effect of both variables on LPH PS producing larger nanoparticulates (Fig 1).

Likewise, the polymer and drug effects on PS, increasing LEC content, significantly, enlarges PS. However, **BC** interaction shows an antagonistic effect on PS (Fig 1). This might be due to the possible attraction between the cationic E and the anionic LEC producing more compact smaller particles [12]. In contrast, the ***stirring speed (D)*** shows a negative effect on PS. The mechanical and hydraulic shear generated by increasing the stirring speed produced ELPH with lower PS [63].

Eq (6) shows a positive correlation between all factors effects and EE % with the highest one being that of the drug amount ***(C)***. Being a hydrophilic drug, increasing E amount enhanced its encapsulation. These results are in agreement with others who reported that EE% enhancement of glibenclamide was directly correlated to the increased drug content[64]. A direct positive effect was also found for ***LEC amount (B)*** on EE %, where the more the lipid content of the bilayer, the more its barrier effect is pronounced, hindering E diffusion from the polymer core [65]. An antagonistic effect of **AB** interaction between the polymer and lipid amounts on drug EE% was seen in Fig 2. Generally, the solubility of drug- polymer mixture into the melted lipid phase is a crucial parameter that determines the drug loading [66]. The miscibility of drug with the formulation components mainly depends on their mutual solubilities and polarities. By virtue of E hydrophilicity (log p -1.11) [67], the milieu is thought to be too hydrophobic to encapsulate it.

The EE% is significantly increased by rising the ***stirring speed (D)***. This might be attributed to the critical turbulent flow time when accompanied with high stirring speeds. In nanoprecipitation, nanoparticles are formed by interfacial phenomena due to the convection effects caused by interfacial turbulence. A physicochemical instability is produced by solvent transport and local regions of supersaturation are formed [68]. It might be assumed that turbulence, applied for a specified time, would enhance the evaporation of the organic solvent preventing drug leakage. Optimum flow rate was also reported during flash precipitation [69].
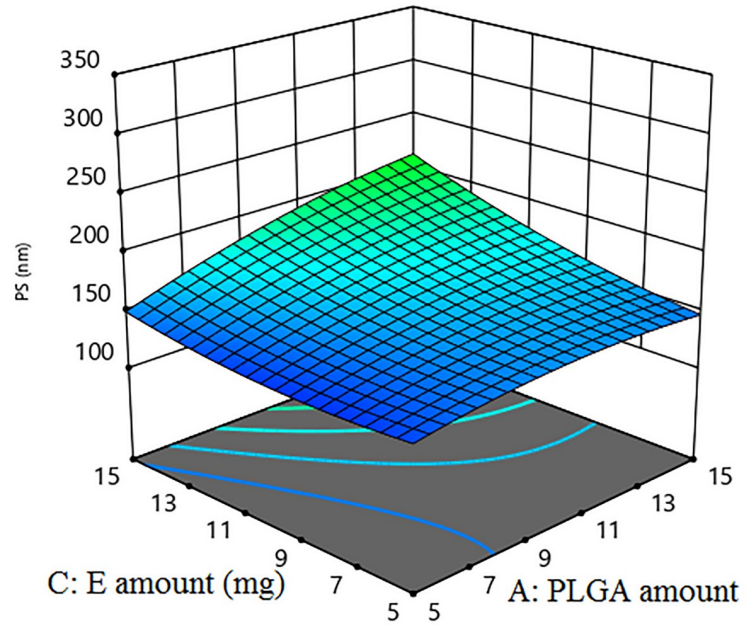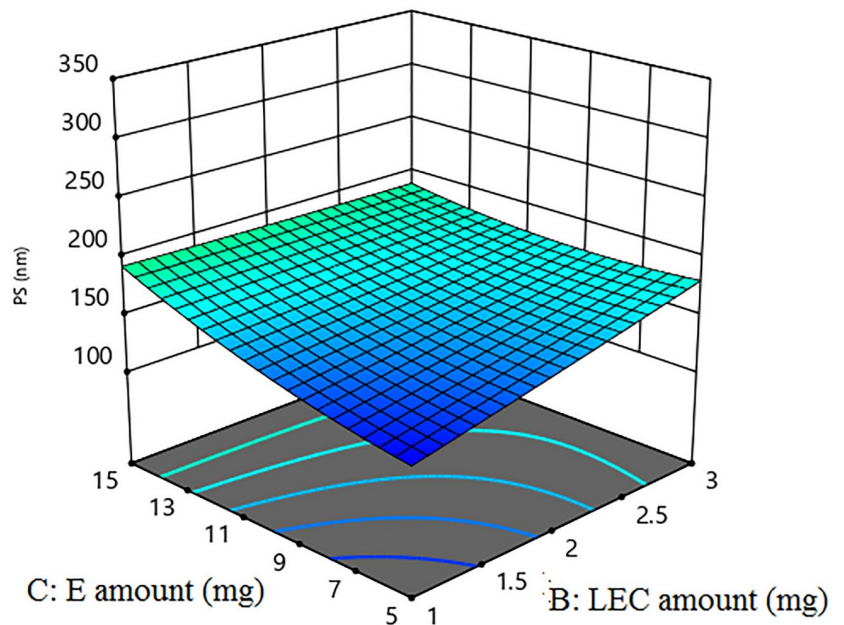
Fig 1. Response 3D plot for the significant parameters interaction on ELPH PS (Y1). Interaction of (AB) between PLGA and E (A). Interaction of (BC) between LEC and E (B). The positive interaction between PLGA and E indicates an enhanced effect of both variables on LPH PS. On the contrary, LEC-E interaction shows an antagonistic effect on PS.

https://doi.org/10.1371/journal.pone.0227231.g001

3.1.2. Design space and optimization. The design space was plotted by overlapping different CPPs influence on CQAs contour plots to obtain QTPP. The yellow area represents the values of CPPs when optimized to fulfill QTPP criteria; minimum PS and maximum EE% (S1 Fig). Based on the high desirability and for model validation, three ELPH (F1-LEC, F2-LEC and F3-LEC) were selected and prepared as checkpoint. Table 2 depicts their compositions, sizes and EE %. It is worth mentioning that the linear correlation plots between experimental

Fig 2. Response 3D plot for the interaction of (AB) between PLGA and LEC on ELPH EE% (Y2). The interaction between the polymer and lipid amounts has a negative influence on drug EE%.

and predicted responses showed R^2 value of 0.9932 and 0.9943 for Y1 and Y2 respectively indicating model suitability.

3.2. Evaluation of optimized ELPH and effect of lipid modification and vitamin E coating

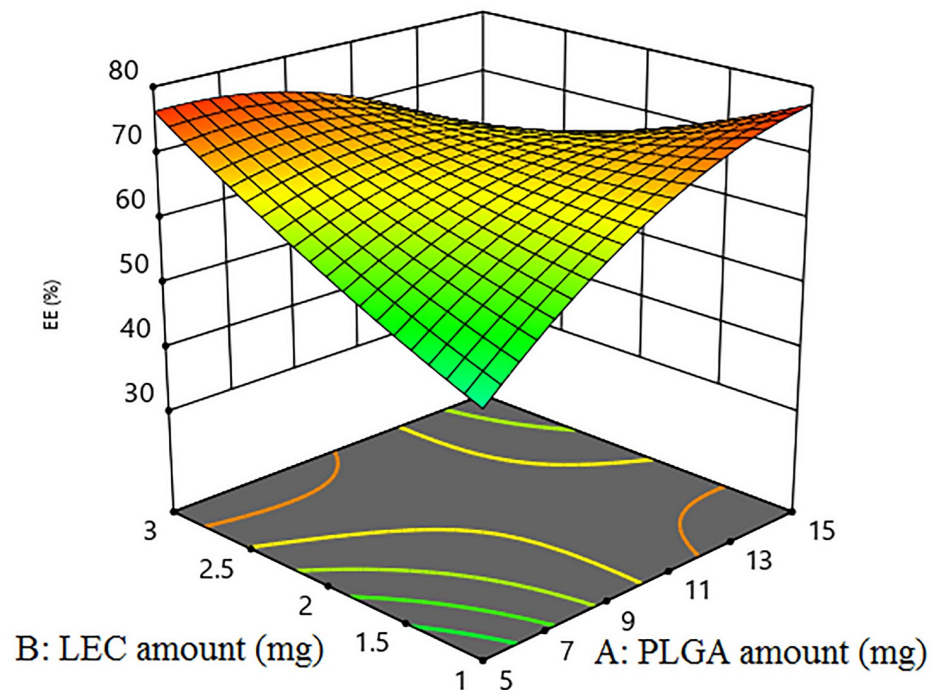Three optimized ELPH were characterized, displaying PS <200 nm, EE% values >75% and **PDI** values below 0.2. The **ξ** values were found to be from -14.51±1.85 to -25.51±2.62 depending on LEC and drug content (Table 3).

Moreover, the **drug LC %** of the optimized formulae ranged from 6.13 to 8.45% (Table 3). This was consistent with previous literature that showed similar LC% for different drugs, when formulated as LPH, such as: ≈9% for amphotericin B [51], 1.8–9% with erlotinib [70] and 8–10% in case of etoposide [71]. It is to be pointed out that though the differences between LC % of the three ELPH (F1-LEC, F2-LEC and F3-LEC) were significantly different ($p > 0.05$), yet the values are not critical from a practical point of view.

3.2.1. Effect of lipid modification on ELPH characteristics. Previous studies had outlined the effect of lipid composition on the physicochemical properties of LPH including drug release [72]. Others have reported that the drug content affected the drug release from LPH [73] and a third group proved a 7 day release for docetaxel sodium from LPH with LEC and GMS as lipid components [74].

Accordingly, various lipid mixtures were tested and tailored to control the drug release from the selected ELPH. Following a preliminary screening, optimized ELPH were prepared using LEC to CH in 1:1.5 ratio and LEC to GMS 1:1, while keeping the total lipid amount

Table 3. Composition and characteristics of the optimized, lipid modified ELPH and vitamin E coated ELPH.

Code	Composition				Lipid composition	LEC / CH or GMS ratio	Characteristics				
	PLGA (mg)	Lipid (mg)	E (mg)	Stirring Speed (rpm)			PS (nm)[c, f, g]	PDI[c, f]	EE%[d, f]	ξ(mV)[c, g]	Drug loading (%)[e, f, g]
ELPH[a, f]											
F1-LEC	5	2.85	13.33	900	LEC		122±5	0.176 ±0.01	81.25±2	-18.26±1	8.45±1
F2-LEC	15	1	9.45	900			128.6±4	0.184±0.02	79.54±3	-14.51±2	6.13±0.3
F3-LEC	5	2.93	9.45	1000			128±5	0.151±0.02	77.12± 2	-25.51±3	6.21±0.2
F1-CH	5	2.85	13.33	900	LEC /CH	1:1.5	166.33±10*	0.154±0.01	79.89±2	-32.51±2*	8.36±0.11
F2-CH	15	1	9.45	900			168.66±6*	0.139±0.02	78.73±3	-25.32±2*	6.02±0.12
F3-CH	5	2.93	9.45	1000			160.33±9*	0.182±0.02	74.26±2	-42.88±1*	5.87± 0.14
F1-GMS	5	2.85	13.33	900	LEC /GMS	1:1	176±8*	0.185±0.02	78.56±2	-38.17±1*	8.48±0.13
F2-GMS	15	1	9.45	900			172.33±3*	0.173±0.02	79.70±2	-29.19±1*	6.02±0.2
F3-GMS	5	2.93	9.45	1000			170±6*	0.167±0.02	79.23±1	-50.19±2*	6.05±0.2
EELPH[b, f]											
F1-GMS/Vit E	5	2.85	13.33	900	LEC /GMS/vit E	1:1	190.66±4*	0.117±0.01	79.73±1	-30.68±2*	7.41±0.2*
F2-GMS/Vit E	15	1	9.45	900			188.66±4*	0.143±0.02	80.47±2	-21.55±1*	5.49±0.2*
F3-GMS/Vit E	5	2.93	9.45	1000			190 ±7*	0.187±0.02	76.11±2	-42.53±3*	5.30±0.4*

[a] ELPH contains LEC, LEC-CH or LEC-GMS as a lipid shell

[b] EELPH is vitamin E coated E loaded GMS LPH

[c] Measured by DLS

[d] Calculated as percentage of initial E added, determined directly by HPLC.

[e] Calculated as percentage of entrapped E weight to the total ELPH or EELPH weight.

[f] Results are expressed as mean ± SD (n = 3).

[g] Statistical analysis was carried out using student's T-test

* $p < 0.05$.

Comparison between lipids modified LPH with LEC-based LPH.

https://doi.org/10.1371/journal.pone.0227231.t003

constant. These formulae were labeled F1-CH, F2-CH and F3-CH for CH modified systems or F1-GMS, F2-GMS and F3-GMS for GMS based ones (Table 3).

Increasing CH or GMS amounts significantly increased the PS of all the fabricated lipid modified ELPH *(p<0.05)*. LPH prepared using lipid combinations were reported to be larger than those prepared using single ones [56]. By comparing the impact of CH and GMS modification on the PS, it could be concluded that GMS based LPH had significantly higher PS than their counterparts, CH based ones (p<0.05). This could be due to the larger molecular area of GMS (40 $A^{\circ 2}$) in comparison to CH (32 $A^{\circ 2}$) [75]. Similarly, the addition of either CH or GMS increased significantly the electronegativity of LPH (p<0.05). The higher absolute ξ values obtained with GMS, might be due to the possible free fatty acids of GMS [76]. In contrast, the incorporation of CH or GMS (Table 3) exhibited non-significant effect on both drug EE% and LC% whatever the composition of the LPH lipid shell (p>0.05).

3.3. Drug release study

The controlled release pattern in nanoparticulate systems is an essential prerequisite for efficient therapeutic outcomes [77], possibly by avoiding the undesirable circulation drug leakage [50]. A feature generally enhanced by LPH due to the barrier effect of the lipid shell [26].

All LPH formulations, prepared using LEC as the sole component of the lipid shell exhibited the same release pattern for 12–18 h (<24 h). (Fig 3A–3C) A release controlled by PLGA and the phospholipid. By applying the similarity factor calculations, F1-LEC and F3-LEC and F2-LEC vs. F3-LEC with respective (*f*2 = 44.55% and 46.84%) exhibited dissimilar release profiles. Accordingly, increasing the drug amount enhances the drug release. On the other hand, increasing polymer content prolonged E release. Additionally, the concomitant increase in PS observed with increasing PLGA content diminish the particles surface area available for drug release [78].

Modified lipid shell of ELPH by lipid variations may reduce the water penetration to the polymeric core, decreasing the polymer hydrolysis rate [19]. Generally, blending either CH or GMS with the LEC in the lipid shell during the fabrication of ELPH presented a more prolonged drug release than that of unmodified LEC based formulae. CH addition caused ~ 100% E release after 36, 48 and 42 h for F1-CH, F2-CH and F3-CH respectively (Fig 3A–3C) in comparison to less than 24 h with the phospholipid alone. Admixing GMS with LEC resulted in more drug release sustainment over 72, 120 and 96 h for the LPHs, F1-GMS, F2-GMS and F3-GMS respectively (Fig 3A–3C).
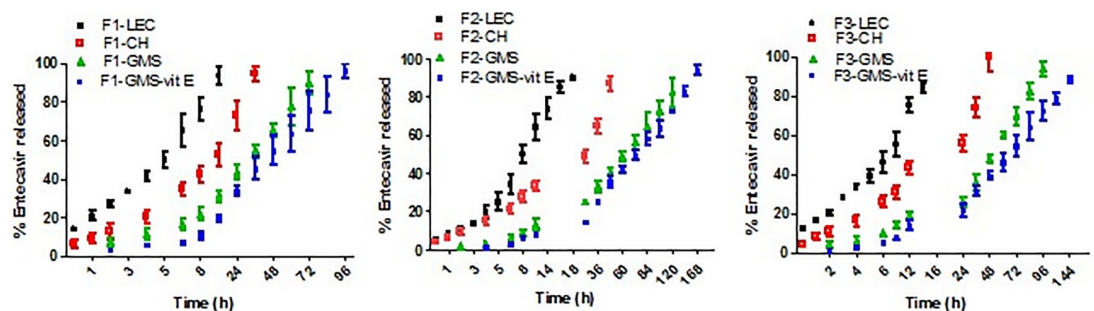
Fig 3. *In vitro* **release profile of drug from different lipid polymer hybrid nanoparticles.** *In vitro* E release from F1 prepared using LEC, LEC-CH, LEC-GMS and vitamin E coated LEC-GMS as lipid shell (A), F2 prepared using LEC, LEC-CH, LEC-GMS and vitamin E coated LEC-GMS as lipid shell (B), F3 prepared using LEC, LEC-CH, LEC-GMS and vitamin E coated LEC-GMS as lipid shell (C) after exposure to 50% final concentration rat serum. E release was measured by dialyzing each formula against PBS (pH 7.4). Drug concentration in the dialysate was quantified by HPLC. Data point represents mean and SD (n = 3).

CH, an essential membrane-stabilizing lipid, has been widely explored in liposome formulations [79]. In addition to its stabilizing effect, CH was found to reduce water permeability through the lipid bilayer [72]. Similarly, the incorporation of GMS increased the LPH hydrophobicity, decreasing the interfacial area between the system and the dissolution medium [80]. Consequently, GMS significantly decreased the E release ($p < 0.05$).

The more prolonged E release from GMS based formulae over CH based ones, could be correlated with the inverse relation between the drug-lipid solubility. Solubility studies show higher drug solubility in GMS, either alone or combined with LEC than in individual CH or CH- LEC mixture (S1 File, S5 Table). The high affinity of the drug to the lipid could hamper the partitioning of E to the dissolution medium as stated earlier [81]. Secondly, GMS was reported to be able of packing with LEC due to hydrophobic interaction between their respective hydrophobic parts and hydrogen bonds between their hydrophilic segments resulting in higher viscosity upon contact with water [82]. Thirdly, the higher PS, attained with GMS modified ELPH, could increase the diffusion path length [83]. in addition, the bigger PS with its smaller the surface area per unit volume available for release [84].

As hypothesized, combined coating of lipid shell (i.e LEC-GMS mixture) and the lipophilic vitamin E could offer more prolonged release prospects. Therefore, ELPH enriched with GMS were surface coated with vitamin E. Vitamin E, is a lipid soluble antioxidant with a partition coefficient 12.18. It exhibits a potent protective and repairing activity against peroxy radical induced biological membrane damage [85]. Moreover, vitamin E could be transferred physiologically from serum to the liver [86]. Hence, E GMS modified LPH were coated with vitamin E by physical adsorption producing EELPH. This could result in drug sustainment with possible stability and bioavailability improvement as described by [87]. Binding of vitamin E to the LEC in the lipid shell could occur via the interaction between the vitamin E phenoxyl hydroxyl group and the LEC phosphate and/or carbonyl group as well-described previously [88].

Successful coating due to the layer deposition on the fabricated systems was proved by a significant increase in PS ($p < 0.05$). These results are in agreement with previous reports which demonstrated PS increase after coating of various NPs e.g.: TPGS coated polystyrene NPs, PEG and chitosan coated PLGA- Vitamin-E-TPGS NPs [87, 89]. The obtained PS and PDI values of the EELPH remained < 200 nm and < 0.2 respectively. Moreover, the ξ. of EELPH formulae was significantly reduced if compared to naked uncoated formulae ($p < 0.05$). This may be attributed to the ability of the coat to shift the shear plane of the diffusion layer to longer distance thus decrease the absolute value of ξ. relative to stern potential [87].

EE% in EELPH did not significantly changed ($p > 0.05$), while LC% exhibited a significant reduction due to mass increase ($p < 0.05$) [70]. Similar results were obtained by Meng and coworkers [90] who explored the inverse relation between the number of coat layers on the PLGA and the loading efficiency of the encapsulated drug. However, the calculated loading efficiency values were still in acceptable range [70].

A more drug sustainment was noticed from all the vitamin E ELPH where about 100% of the drug was liberated after 96, 168 and 144 h with minimal burst effect from F1-GMS-vit E, F2-GMS-vit E and F3-GMS-vit E respectively (Fig 3A–3C). Vitamin E coat provided an additional partial lipophilic barricade on the LPH surface, offering steric force to E diffusion to the release medium [91]. It could be concluded that the approach of lipid coat tuning was efficient to control drug release for one week.

Therefore, formula vitamin E coated F2-GMS (will be referred as EELPH), showing the highest E retardation over one week, was selected for further characterization studies.
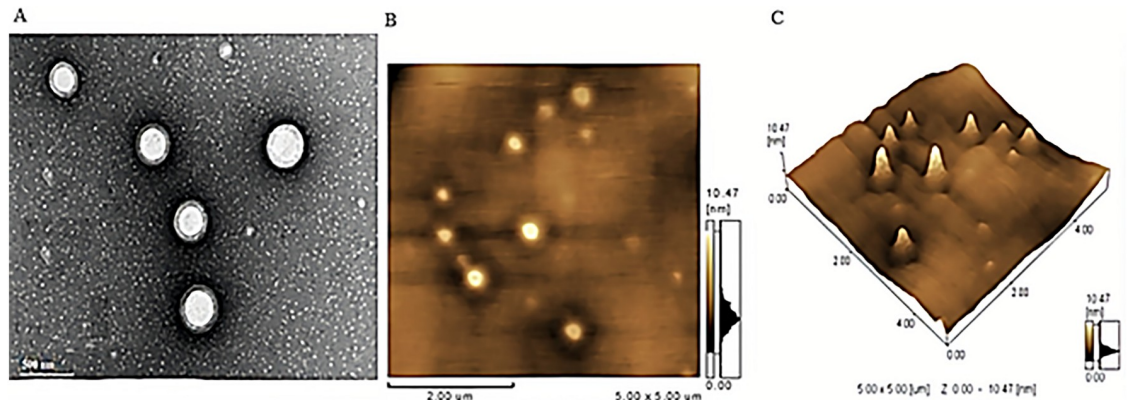
Fig 4. Morphological characterization of the optimized EELPH. Transmission electron micrograph (A), Atomic force micrograph planner view (B) and 3-D view (C) of EELPH. EELPH appeared as core-shell nanostructure with PS in consistency with DLS technique.

3.4. Morphological studies

A representative TEM of the selected EELPH is illustrated in Fig 4A. Spherical non-aggregated particles with a PS in the range of 180–190 nm could be seen in the TEM which is consistent with the DLS measurements. The photomicrograph demonstrated the core-shell structure of the coated LPH. The white core in the center is the PLGA core while the gray ring around the polymer core is the coat "lipid shell" [70].

A core-shell structure of EELPH could be depicted from AFM Fig 4B. Moreover, the 3-D structure showed district particles with a PS in accordance with both TEM and DLS (Fig 4C).

3.5. *In vitro* serum stability assay

The colloidal stability of the chosen EELPH was tested in 10% and 50% v/v FBS at 37 ˚C for 4 and 24 h. As shown in Fig 5A–5C, the formula was stable in 10% and 50% v/v FBS as proved by non-significant effect on PS, PDI and ξ at all tested time points ($p > 0.05$). The negligible effect of serum proteins could be ascribed by the electrostatic repulsion between the negatively charged LPH with the serum proteins [50, 92].

3.6. *In vitro* hemolytic assay

The biocompatibility of the fabricated EELPH was assessed by the *in vitro* hemolytic assay. The hemolytic activity was found to be heightened by a concomitant increase in the EELPH concentration. However, the calculated % hemolysis was < 5% in all tested quantities (Fig 6). Previous reports indicated that the accepted limit of hemolysis is from 5% to 25% [93]. However, the new consensus ASTM E2524-08 -Standard test method for analysis of hemolytic properties of nanoparticles limited the threshold to 5% [94]. The safety of NPs coated with vitamin E was reported by many previous studies [94, 95].

3.7. Shelf life colloidal stability study

The selected formula kept its original color with no phase separation or turbidity. No significant change (*p>0.05*) in the PS, PDI, ξ .or EE% was seen after 1, 3 and 6 months storage at 5˚C at different time intervals (Table 4). It is worth noting that as stated earlier, following storage of LPH nanoparticles at climatic conditions of room temperature (25˚C) over a period of 6 months, dramatic changes in the physicochemical properties of the hybrid particles, aggregates
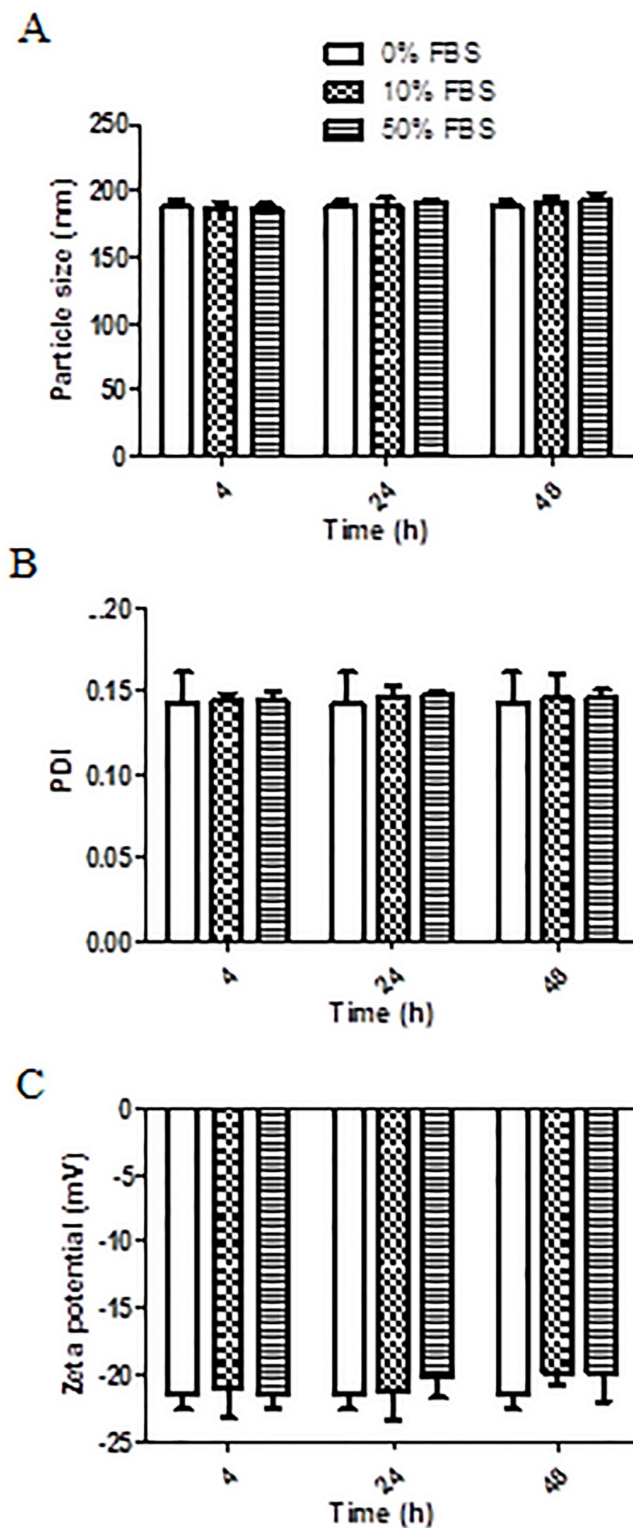
Fig 5. The effect of serum incubation on EELPH PS, PDI and ξ. The selected EELPH were incubated with 0%, 10% and 50% FBS for 4, 24 and 48h then PS (A), PDI (B) and ξ. (C) were measured using DLS as described. Data points represent mean and SD (n = 3). Statistical analysis was carried out using one-way ANOVA followed by Tukey HSD test and $P < 0.05$ was considered significant. Serum protein had a non-significant effect on LPH PS, PDI or ξ.
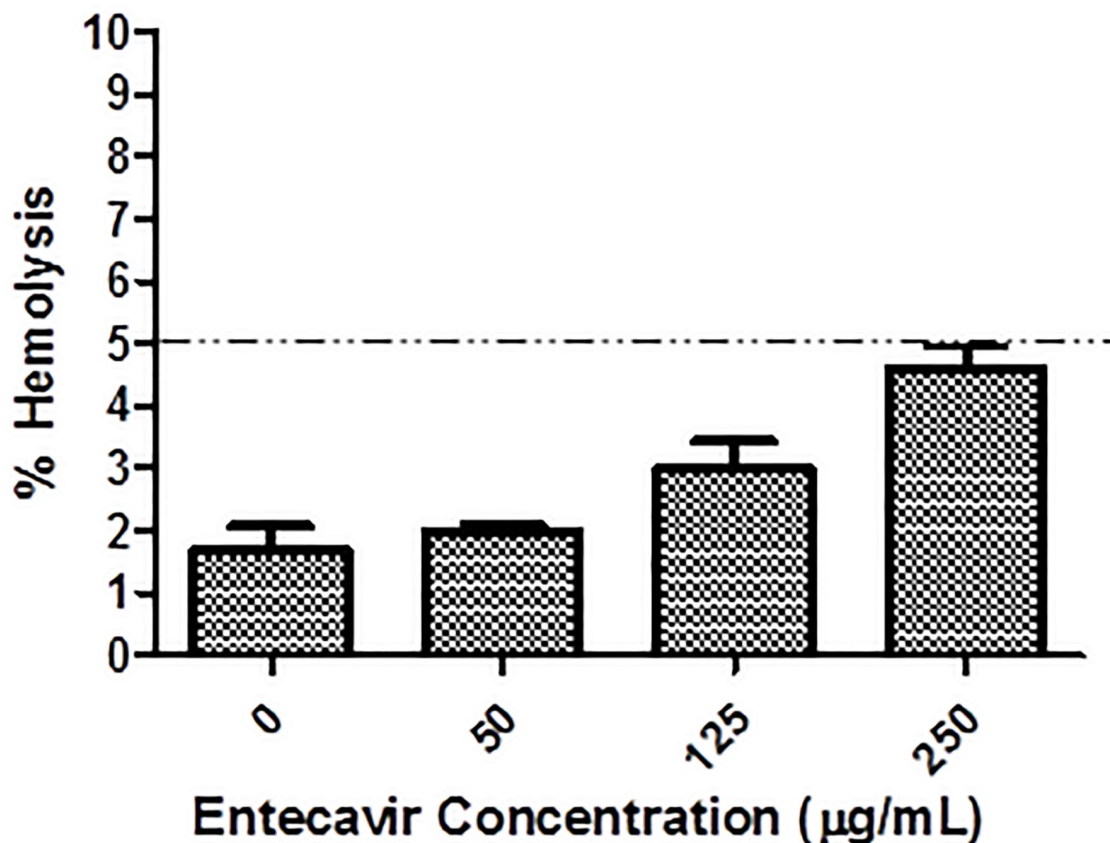
Fig 6. The *in vitro* hemolysis assay of EELPH. Rat RBCs were incubated with EELPH at different E concentrations (0–250 µg/mL) for 2 h at 37˚C. Positive and negative controls were 0.5 w/v% Triton X-100 and PBS (pH 7.4), respectively. Samples were centrifuged at 4000 rpm for 5 min at 4 ˚C and the absorbance of the released haemoglobin was determined at 545 nm. Results are expressed as mean ± SD (n = 3). The dotted line represents the acceptable hemolysis range.

formation, degradation and possible corruption were noticed, signifying the necessity of keeping the storage temperature of LPH at 5˚C [96].

3.8. The effect of vitamin E coating on the cellular uptake of ELPH

High cell viability exceeding 80% was obtained up to a concentration equivalent to 100 µM E for the tested ELPH with or without vitamin E coating (Fig 7). The viability of cells treated

Table 4. Characteristics of the selected EELPH at various time intervals following storage at 5˚C over a 6 months period.

Parameter	Freshly prepared	Storage at 5 ˚C		
		1 month	3 month	6 month
PS (nm) [a, c, d]	188.66±4	185.26±5	183.58±1.5	185.57±1
PDI [a, c, d]	0.143±0.02	0.143± 0.01	0.155±0.01	0.148±0.01
ξ. (mV) [a, c, d]	-21.55±1	-20.69± 2	-20.96±1	-20.79±2
EE% [b, c, d]	80.47±2	80.57±2	79.71±1	81.51±2

[a] Measured by DLS.

[b] Calculated as percentage of initial E added, determined directly by HPLC.

[c] Expressed as mean ± SD (n = 3).

[d] Statistical analysis was carried out using one-way ANOVA followed by Tukey HSD test and $P<0.05$ was considered significant.
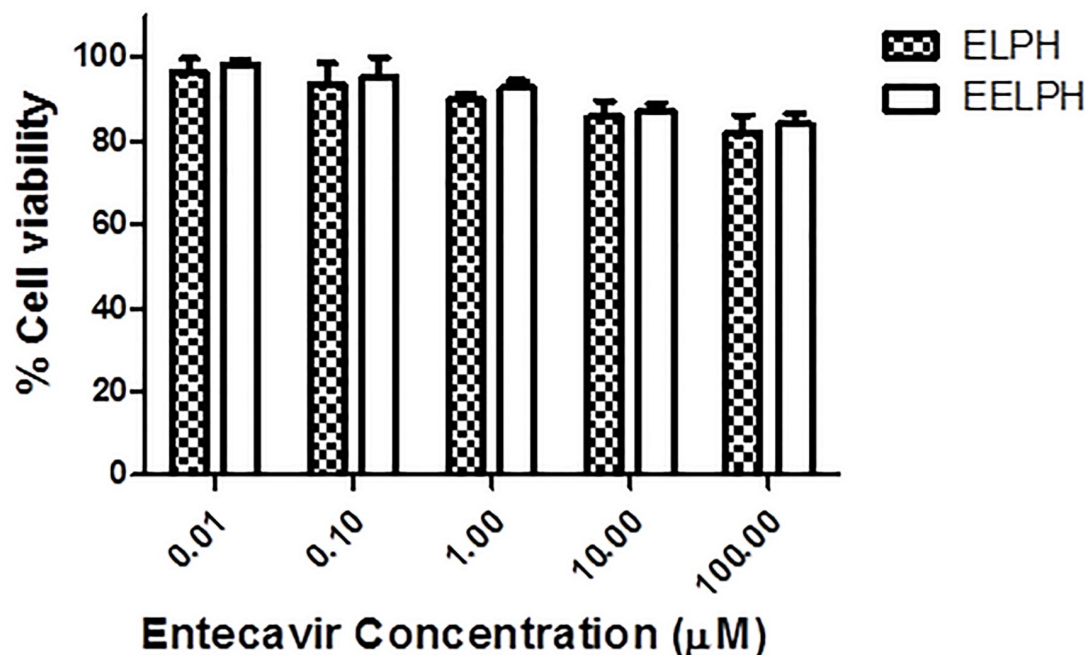
Fig 7. Cell viability assay of ELPH and EELPH after incubation for 48h. J774 macrophage cells were incubated with either ELPH or EELPH at increasing E concentrations (0.01–100 μM). Cells viability were assessed by MTT assay and results are presented as a percentage of the viable cells to the control untreated cells. Both tested formulae showed highe cell viability at all tested E concentrations. Data points are expressed as mean ± SD (n = 5).

with either ELPH or EELPH was significantly higher than that treated with sodium lauryl sulfate at the same concentration (P< 0.05).

Meaningful association between the *in vitro* phagocytosis of delivery nanoplatforms by macrophage and the *in vivo* liver retention is well-addressed [52]. In light of this, internalization of DiI-labelled EELPH (50 nM) in J774 cells was investigated qualitatively by CLSM. Due to the crucial potential of incubation time, boosting the cellular uptake efficiency [97], the cells
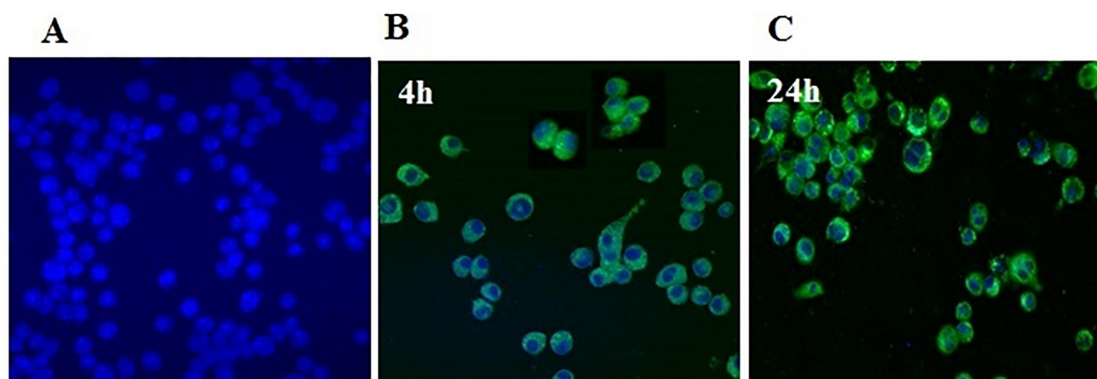
Fig 8. *In vitro* intracellular uptake of EELPH in J774 by confocal laser scanning microscopy. EELPH uptake was assessed by incubating J774 macrophage cells with 50 nM DiI-labelled EELPH for 4 h and 24. Untreated J774 cells appeared as blue due to the staining of the nucleus by DAPI (A), J774 cells treated with 50 nM DiI-labelled EELPH for 4 h (B) and 24 h (C). The uptake was confirmed by green fluorescence inside the cells while the cell nuclei appeared as blue due to the counterstaining with DAPI. The fluorescence intensity was increased in time-dependant manner.
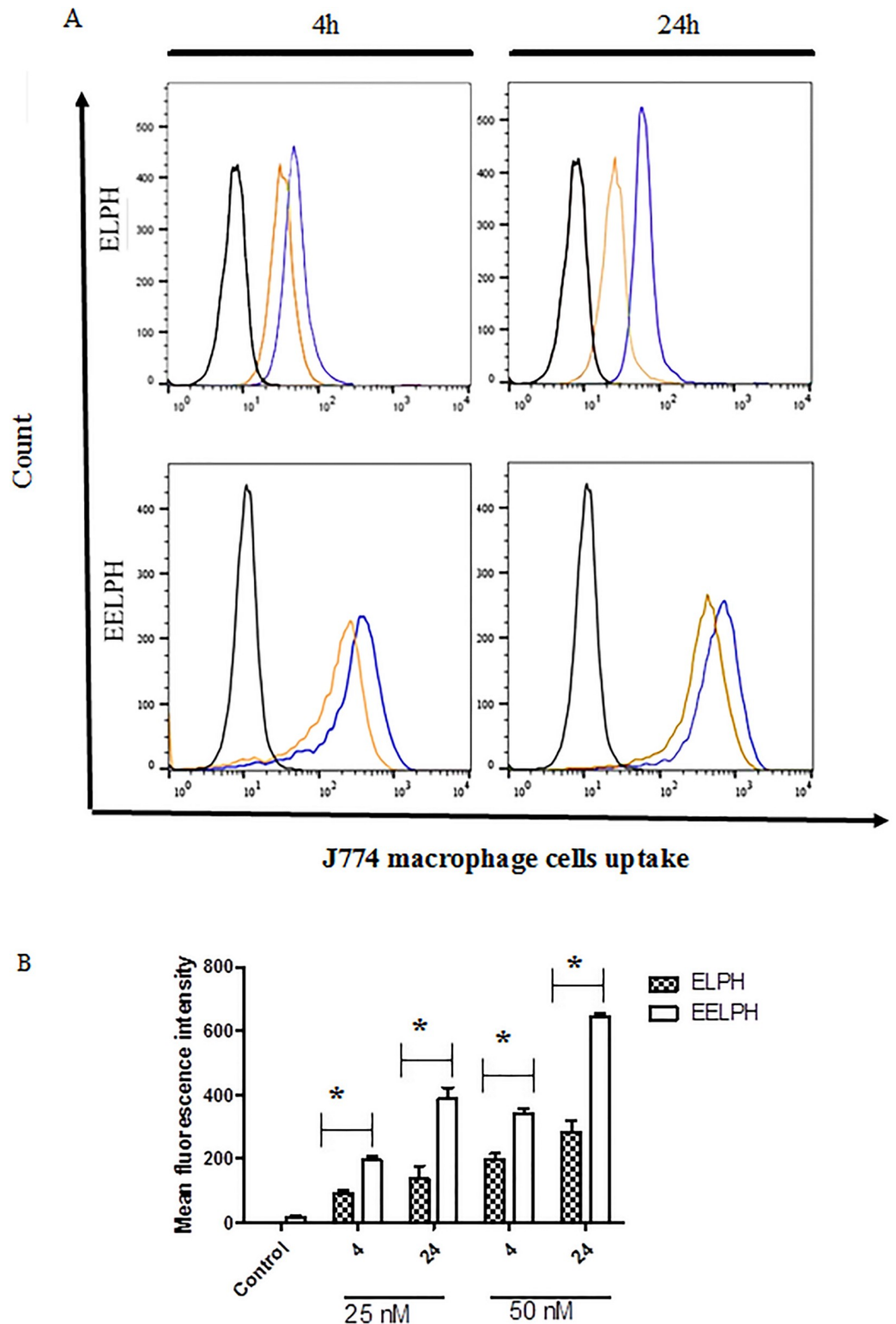
Fig 9. Intracellular uptake of ELPH and EELPH in J774 macrophage cells by flow cytometry. Cells were incubated with DiI-labelled ELPH or EELPH at 25 (brown) or 50 nM (blue) for 4 h or 24 h. Flow cytometry histogram for uptake of DiI-labelled ELPH and EELPH (A). Cellular uptake was quantified by mean florescence intensity (MFI) using flow cytometry and FL-2 detector (B). LPH uptake was higher for EELPH than ELPH and was shown to be dose- and time-dependent. Data points represent mean and SD (n = 3). Statistical analysis was carried out using one-way ANOVA followed by Tukey HSD test and $P{<}0.05$ was considered significant.

were treated with coated LPH, considering two incubation times (4h and 24h). The DiI-labelled EELPH displayed green fluorescence, while J774 cells' nuclei, stained with DAPI, showed blue fluorescence. Expectedly, enhanced time-dependent fluorescence intensity in the cytoplasm of J774 cells was exhibited (Fig 8), indicating meaningful retention efficiency in the cells and subsequent therapeutic efficacy of E [70].

The intracellular internalization of DiI-labelled EELPH was further quantitatively assessed by flow cytometry. Moreover, in order to inspect the effect of vitamin E coating on the cellular uptake, cells were incubated with either EELPH or its uncoated counterpart ELPH (F2-GMS). Control J774 cells, without treatment, displayed auto fluorescence that was highly intensified following treatment of cells with DiI-labelled ELPH or EELPH in both time and concentration-dependent manners (Fig 9A).

As displayed in Fig 9B, increasing the concentration of either ELPH or EELPH from 25 to 50 nM yielded ≈1.5–2 fold increase in the mean fluorescence intensity (MFI) after 4 h. Meanwhile prolonging the incubation period to 24 h demonstrated ≈2 fold in the measured MFI. In addition, EELPH exhibited a significant 1.7–2 fold increase in the measured MFI values over the uncoated one. The presence of vitamin E significantly improved the cellular uptake efficiency by the macrophages (p< 0.05). This could be attributed to the potential ability of vitamin E to stimulate the phagocytic activity of macrophage as immunomodulatory to improve the phagocytic activity of macrophage as mentioned early [41].

4. Conclusion

HBV infection was considered as a major cause of death worldwide, due to the risk of cirrhosis, hepatocellular cancer, portal hypertension and liver failure. E monotherapy have been suggested for 48 weeks. Hence, the study offers a long-acting parenteral LPH of E. A platform, which combines the benefits of both polymeric and lipid carriers. The lipid shell was modulated with GMS to extend the drug release followed by Vitamin E coating to enhance liver targeting with more hydrophobic barriers for drug liberation. The optimized vitamin E coated LPH with LEC-GMS shell displayed favorable PS (188.66 nm) for passive targeting, an E entrapment of 80.47% and sustained release for one week. In addition, ELPH coated with vitamin E proved an increased in vitro macrophage retention, in comparison to the uncoated ones. In vivo antiviral activity should be considered in the future.

Supporting information

S1 Fig. Overlay plots depicting the design space region for the optimized ELPH. The design space was plotted by overlapping different CPPs influence on CQAs contour plots to obtain QTPP. The yellow area represents the values of CPPs when optimized to fulfill QTPP criteria; minimum PS (< 200 nm) and maximum EE%.
(TIF)

S1 File.
(DOCX)

S1 Table. Model summary statistics for particle size (Y1).
(DOCX)

S2 Table. Model summary statistics for entrapment efficiency (Y2).
(DOCX)

S3 Table. ANOVA of the obtained data from BBD for the particle size of ELPH.
(DOCX)

S4 Table. ANOVA for the encapsulation efficiency for ELPH.
(DOCX)

S5 Table. Solubility of E in the utilized individual lipids and their combinations.
(DOCX)

Author Contributions

Formal analysis: Mohamed Hamdi, Gehanne A. S. Awad.

Investigation: Mohamed Hamdi, Hend Mohamed Abdel-Bar, Enas Elmowafy.

Methodology: Mohamed Hamdi, Hend Mohamed Abdel-Bar.

Resources: Khuloud T. Al-Jamal.

Supervision: Gehanne A. S. Awad.

Writing – original draft: Enas Elmowafy.

Writing – review & editing: Khuloud T. Al-Jamal, Gehanne A. S. Awad.

References

1. Boltjes A, Movita D, Boonstra A, Woltman AM. The role of Kupffer cells in hepatitis B and hepatitis C virus infections. Journal of hepatology. 2014; 61(3):660–71. https://doi.org/10.1016/j.jhep.2014.04.026 PMID: 24798624

2. Faure-Dupuy S, Durantel D, Lucifora J. Liver macrophages: Friend or foe during hepatitis B infection? Liver international. 2018; 38(10):1718–29. https://doi.org/10.1111/liv.13884 PMID: 29772112

3. Ju C, Tacke F. Hepatic macrophages in homeostasis and liver diseases: from pathogenesis to novel therapeutic strategies. Cellular & molecular immunology. 2016; 13(3):316.

4. Li L, Wang H, Ong ZY, Xu K, Ee PLR, Zheng S, et al. Polymer-and lipid-based nanoparticle therapeutics for the treatment of liver diseases. Nano today. 2010; 5(4):296–312.

5. Singh L, Indermun S, Govender M, Kumar P, du Toit L, Choonara Y, et al. Drug delivery strategies for antivirals against hepatitis B virus. Viruses. 2018; 10(5):267.

6. Zhang C, Wang A, Wang H, Yan M, Liang R, He X, et al. Entecavir-loaded poly (lactic-co-glycolic acid) microspheres for long-term therapy of chronic hepatitis-B: Preparation and in vitro and in vivo evaluation. International journal of pharmaceutics. 2019; 560:27–34. https://doi.org/10.1016/j.ijpharm.2019.01.052 PMID: 30711615

7. Singh L, Kruger HG, Maguire GE, Govender T, Parboosing R. The role of nanotechnology in the treatment of viral infections. Therapeutic advances in infectious disease. 2017; 4(4):105–31. https://doi.org/10.1177/2049936117713593 PMID: 28748089

8. He S, Lin Q, Qu M, Wang L, Deng L, Xiao L, et al. Liver-targeted co-delivery of entecavir and glycyrrhetinic acid based on albumin nanoparticle to enhance the accumulation of entecavir. Molecular pharmaceutics. 2018; 15(9):3953–61. https://doi.org/10.1021/acs.molpharmaceut.8b00408 PMID: 30110554

9. Wu X, Zhou J, Xie W, Ding H, Ou X, Chen G, et al. Entecavir monotherapy versus de novo combination of lamivudine and adefovir for compensated hepatitis B virus-related cirrhosis: a real-world prospective multicenter cohort study. Infection and drug resistance. 2019; 12:745. https://doi.org/10.2147/IDR.S185120 PMID: 31015765

10. Yokosuka O, Takaguchi K, Fujioka S, Shindo M, Chayama K, Kobashi H, et al. Long-term use of entecavir in nucleoside-naive Japanese patients with chronic hepatitis B infection. Journal of hepatology. 2010; 52(6):791–9. https://doi.org/10.1016/j.jhep.2009.12.036 PMID: 20409606

11. Zoutendijk R, Reijnders JG, Brown A, Zoulim F, Mutimer D, Deterding K, et al. Entecavir treatment for chronic hepatitis B: adaptation is not needed for the majority of naive patients with a partial virological response. Hepatology. 2011; 54(2):443–51. https://doi.org/10.1002/hep.24406 PMID: 21563196

12. Lim J-L, Ki M-H, Joo MK, An S-W, Hwang K-M, Park E-S. An injectable liquid crystal system for sustained delivery of entecavir. International journal of pharmaceutics. 2015; 490(1–2):265–72. https://doi.org/10.1016/j.ijpharm.2015.05.049 PMID: 26004002

13. Ho MJ, Lee DR, Im SH, Yoon JA, Shin CY, Kim HJ, et al. Microsuspension of fatty acid esters of entecavir for parenteral sustained delivery. International journal of pharmaceutics. 2018; 543(1–2):52–9. https://doi.org/10.1016/j.ijpharm.2018.03.042 PMID: 29597034

14. Tahir N, Madni A, Balasubramanian V, Rehman M, Correia A, Kashif PM, et al. Development and optimization of methotrexate-loaded lipid-polymer hybrid nanoparticles for controlled drug delivery applications. International journal of pharmaceutics. 2017; 533(1):156–68. https://doi.org/10.1016/j.ijpharm.2017.09.061 PMID: 28963013

15. Thanki K, Zeng X, Justesen S, Tejlmann S, Falkenberg E, Van Driessche E, et al. Engineering of small interfering RNA-loaded lipidoid-poly (DL-lactic-co-glycolic acid) hybrid nanoparticles for highly efficient and safe gene silencing: A quality by design-based approach. European journal of pharmaceutics and biopharmaceutics. 2017; 120:22–33. https://doi.org/10.1016/j.ejpb.2017.07.014 PMID: 28756280

16. Huo ZJ, Wang SJ, Wang ZQ, Zuo WS, Liu P, Pang B, et al. Novel nanosystem to enhance the antitumor activity of lapatinib in breast cancer treatment: therapeutic efficacy evaluation. Cancer science. 2015; 106(10):1429–37. https://doi.org/10.1111/cas.12737 PMID: 26177628

17. Allen TM, Cullis PR. Liposomal drug delivery systems: from concept to clinical applications. Advanced drug delivery reviews. 2013; 65(1):36–48. https://doi.org/10.1016/j.addr.2012.09.037 PMID: 23036225

18. Dehaini D, Fang RH, Luk BT, Pang Z, Hu C-MJ, Kroll AV, et al. Ultra-small lipid–polymer hybrid nanoparticles for tumor-penetrating drug delivery. Nanoscale. 2016; 8(30):14411–9. https://doi.org/10.1039/c6nr04091h PMID: 27411852

19. Hadinoto K, Sundaresan A, Cheow WS. Lipid–polymer hybrid nanoparticles as a new generation therapeutic delivery platform: a review. European journal of pharmaceutics and biopharmaceutics. 2013; 85(3):427–43.

20. Bose RJ, Ravikumar R, Karuppagounder V, Bennet D, Rangasamy S, Thandavarayan RA. Lipid–polymer hybrid nanoparticle-mediated therapeutics delivery: advances and challenges. Drug discovery today. 2017; 22(8):1258–65. https://doi.org/10.1016/j.drudis.2017.05.015 PMID: 28600191

21. Chaudhary Z, Ahmed N, ur. Rehman A, Khan GM. Lipid polymer hybrid carrier systems for cancer targeting: a review. International journal of polymeric materials and polymeric biomaterials. 2018; 67(2):86–100.

22. Ana R, Mendes M, Sousa J, Pais A, Falcão A, Fortuna A, et al. Rethinking carbamazepine oral delivery using polymer-lipid hybrid nanoparticles. International journal of pharmaceutics. 2019; 554:352–65. https://doi.org/10.1016/j.ijpharm.2018.11.028 PMID: 30439493

23. Silva EJ, Souza LG, Silva LA, Taveira SF, Guilger RC, Liao LM, et al. A novel polymer-lipid hybrid nanoparticle for the improvement of topotecan hydrochloride physicochemical properties. Current drug delivery. 2018; 15(7):979–86. https://doi.org/10.2174/1567201815666171215110026 PMID: 29243576

24. Li A, Yang F, Xin J, Bai X. An efficient and long-acting local anesthetic: ropivacaine-loaded lipid-polymer hybrid nanoparticles for the control of pain. International journal of nanomedicine. 2019; 14:913. https://doi.org/10.2147/IJN.S190164 PMID: 30774342

25. Liang J, Liu Y, Liu J, Li Z, Fan Q, Jiang Z, et al. Chitosan-functionalized lipid-polymer hybrid nanoparticles for oral delivery of silymarin and enhanced lipid-lowering effect in NAFLD. Journal of nanobiotechnology. 2018; 16(1):64. https://doi.org/10.1186/s12951-018-0391-9 PMID: 30176941

26. Date T, Nimbalkar V, Kamat J, Mittal A, Mahato RI, Chitkara D. Lipid-polymer hybrid nanocarriers for delivering cancer therapeutics. Journal of controlled release. 2018; 271:60–73. https://doi.org/10.1016/j.jconrel.2017.12.016 PMID: 29273320

27. Zhang L, Zhang L. Lipid–polymer hybrid nanoparticles: synthesis, characterization and applications. Nano life. 2010; 1(01n02):163–73.

28. Danhier F, Ansorena E, Silva JM, Coco R, Le Breton A, Préat V. PLGA-based nanoparticles: an overview of biomedical applications. Journal of controlled release. 2012; 161(2):505–22. https://doi.org/10.1016/j.jconrel.2012.01.043 PMID: 22353619

29. Chen L-C, Chen Y-C, Su C-Y, Wong W-P, Sheu M-T, Ho H-O. Development and characterization of lecithin-based self-assembling mixed polymeric micellar (saMPMs) drug delivery systems for curcumin. Scientific reports. 2016; 6:37122. https://doi.org/10.1038/srep37122 PMID: 27848996

30. Jin X, Zhang Z-H, Sun E, Tan X-B, Zhu F-X, Jia X-B. A novel drug–phospholipid complex loaded micelle for baohuoside I enhanced oral absorption: in vivo and in vivo evaluations. Drug development and industrial pharmacy. 2013; 39(9):1421–30. https://doi.org/10.3109/03639045.2012.719234 PMID: 23057574

31. Yanasarn N, Sloat BR, Cui Z. Nanoparticles engineered from lecithin-in-water emulsions as a potential delivery system for docetaxel. International journal of pharmaceutics. 2009; 379(1):174–80. https://doi.org/10.1016/j.ijpharm.2009.06.004 PMID: 19524029

32. Briuglia M-L, Rotella C, McFarlane A, Lamprou DA. Influence of cholesterol on liposome stability and on in vitro drug release. Drug delivery and translational research. 2015; 5(3):231–42. https://doi.org/10.1007/s13346-015-0220-8 PMID: 25787731

33. Maboos M, Yousuf RI, Shoaib MH, Nasiri I, Hussain T, Ahmed HF, et al. Effect of lipid and cellulose based matrix former on the release of highly soluble drug from extruded/spheronized, sintered and compacted pellets. Lipids in health and disease. 2018; 17(1):136. https://doi.org/10.1186/s12944-018-0783-8 PMID: 29885655

34. Magarkar A, Dhawan V, Kallinteri P, Viitala T, Elmowafy M, Róg T, et al. Cholesterol level affects surface charge of lipid membranes in saline solution. Scientific reports. 2014; 4:5005. https://doi.org/10.1038/srep05005 PMID: 24845659

35. Gardouh AR, Gad S, Ghonaim HM, Ghorab MM. Design and characterization of glyceryl monostearate solid lipid nanoparticles prepared by high shear homogenization. British journal of pharmaceutical research. 2013; 3(3):326.

36. Kumar R, Yasir M, Saraf SA, Gaur PK, Kumar Y, Singh AP. Glyceryl monostearate based nanoparticles of mefenamic acid: fabrication and in vitro characterization. Drug invention today. 2013; 5(3):246–50.

37. Uppulurj KB. Self nano emulsifying drug delivery systems for oral delivery of hydrophobic drugs. Biomedical and pharmacology journal. 2015; 6(2):355–62.

38. Traber MG. Vitamin E regulatory mechanisms. Annu Rev Nutr. 2007; 27:347–62. https://doi.org/10.1146/annurev.nutr.27.061406.093819 PMID: 17439363

39. Lewis ED, Meydani SN, Wu D. Regulatory role of vitamin E in the immune system and inflammation. IUBMB life. 2019; 71(4):487–94. https://doi.org/10.1002/iub.1976 PMID: 30501009

40. Konjufca V, Bottje W, Bersi T, Erf G. Influence of dietary vitamin E on phagocytic functions of macrophages in broilers. Poultry science. 2004; 83(9):1530–4. https://doi.org/10.1093/ps/83.9.1530 PMID: 15384903

41. Zingg J-M. Vitamin E: an overview of major research directions. Molecular aspects of medicine. 2007; 28(5–6):400–22. https://doi.org/10.1016/j.mam.2007.05.004 PMID: 17624418

42. Nishina K, Unno T, Uno Y, Kubodera T, Kanouchi T, Mizusawa H, et al. Efficient in vivo delivery of siRNA to the liver by conjugation of α-tocopherol. Molecular therapy. 2008; 16(4):734–40.

43. Das S, Ng WK, Kanaujia P, Kim S, Tan RB. Formulation design, preparation and physicochemical characterizations of solid lipid nanoparticles containing a hydrophobic drug: effects of process variables. Colloids and surfaces b: biointerfaces. 2011; 88(1):483–9. https://doi.org/10.1016/j.colsurfb.2011.07.036 PMID: 21831615

44. Shah B, Khunt D, Bhatt H, Misra M, Padh H. Application of quality by design approach for intranasal delivery of rivastigmine loaded solid lipid nanoparticles: effect on formulation and characterization parameters. European journal of pharmaceutical sciences. 2015; 78:54–66. https://doi.org/10.1016/j.ejps.2015.07.002 PMID: 26143262

45. Emami J, Boushehri MS, Varshosaz J. Preparation, characterization and optimization of glipizide controlled release nanoparticles. Research in pharmaceutical sciences. 2014; 9(5):301. PMID: 25657802

46. Leng D, Thanki K, Fattal E, Foged C, Yang M. Engineering of budesonide-loaded lipid-polymer hybrid nanoparticles using a quality-by-design approach. International journal of pharmaceutics. 2018; 548 (2):740–6. https://doi.org/10.1016/j.ijpharm.2017.08.094 PMID: 28847667

47. El-Gogary RI, Rubio N, Wang JT-W, Al-Jamal WT, Bourgognon M, Kafa H, et al. Polyethylene glycol conjugated polymeric nanocapsules for targeted delivery of quercetin to folate-expressing cancer cells in vitro and in vivo. ACS nano. 2014; 8(2):1384–401. https://doi.org/10.1021/nn405155b PMID: 24397686

48. Shah VP, Tsong Y, Sathe P, Liu J-P. In vitro dissolution profile comparison—statistics and analysis of the similarity factor, f2. Pharmaceutical research. 1998; 15(6):889–96. https://doi.org/10.1023/a:1011976615750 PMID: 9647355

49. Tamilselvan N, Raghavan CV. Formulation and characterization of anti alzheimer's drug loaded chitosan nanoparticles and its in vitro biological evaluation. Journal of young pharmacists. 2015; 7(1):28.

50. Zhao X, Li F, Li Y, Wang H, Ren H, Chen J, et al. Co-delivery of HIF1α siRNA and gemcitabine via biocompatible lipid-polymer hybrid nanoparticles for effective treatment of pancreatic cancer. Biomaterials. 2015; 46:13–25. https://doi.org/10.1016/j.biomaterials.2014.12.028 PMID: 25678112

51. Asthana S, Jaiswal AK, Gupta PK, Dube A, Chourasia MK. Th-1 biased immunomodulation and synergistic antileishmanial activity of stable cationic lipid–polymer hybrid nanoparticle: biodistribution and toxicity assessment of encapsulated amphotericin B. European journal of pharmaceutics and biopharmaceutics. 2015; 89:62–73. https://doi.org/10.1016/j.ejpb.2014.11.019 PMID: 25477079

52. Sato Y, Hatakeyama H, Sakurai Y, Hyodo M, Akita H, Harashima H. A pH-sensitive cationic lipid facilitates the delivery of liposomal siRNA and gene silencing activity in vitro and in vivo. Journal of controlled release. 2012; 163(3):267–76. https://doi.org/10.1016/j.jconrel.2012.09.009 PMID: 23000694

53. Joshi SA, Chavhan SS, Sawant KK. Rivastigmine-loaded PLGA and PBCA nanoparticles: preparation, optimization, characterization, in vitro and pharmacodynamic studies. European journal of pharmaceutics and biopharmaceutics. 2010; 76(2):189–99. https://doi.org/10.1016/j.ejpb.2010.07.007 PMID: 20637869

54. Klippstein R, Wang JTW, El-Gogary RI, Bai J, Mustafa F, Rubio N, et al. Passively targeted curcumin-loaded pegylated PLGA nanocapsules for colon cancer therapy in vivo. Small. 2015; 11(36):4704–22. https://doi.org/10.1002/smll.201403799 PMID: 26140363

55. Hodgins NO, Wang JT-W, Klippstein R, Costa PM, Sosabowski JK, Marshall JF, et al. Investigating in vitro and in vivo αvβ6 integrin receptor-targeting liposomal alendronate for combinatory γδ T cell immunotherapy. Journal of controlled release. 2017; 256:141–52. https://doi.org/10.1016/j.jconrel.2017.04.025 PMID: 28432037

56. Mukherjee A, Waters AK, Kalyan P, Achrol AS, Kesari S, Yenugonda VM. Lipid–polymer hybrid nanoparticles as a next-generation drug delivery platform: state of the art, emerging technologies, and perspectives. International journal of nanomedicine. 2019; 14:1937. https://doi.org/10.2147/IJN.S198353 PMID: 30936695

57. Sylvester B, Porfire A, Achim M, Rus L, Tomuță I. A step forward towards the development of stable freeze-dried liposomes: a quality by design approach (QbD). Drug development and industrial pharmacy. 2018; 44(3):385–97. https://doi.org/10.1080/03639045.2017.1395457 PMID: 29098869

58. Nam HY, Kwon SM, Chung H, Lee S-Y, Kwon S-H, Jeon H, et al. Cellular uptake mechanism and intracellular fate of hydrophobically modified glycol chitosan nanoparticles. Journal of controlled release. 2009; 135(3):259–67. https://doi.org/10.1016/j.jconrel.2009.01.018 PMID: 19331853

59. Kashif PM, Madni A, Ashfaq M, Rehman M, Mahmood MA, Khan MI, et al. Development of Eudragit RS 100 microparticles loaded with ropinirole: optimization and in vitro evaluation studies. AAPS pharmscitech. 2017; 18(5):1810–22. https://doi.org/10.1208/s12249-016-0653-5 PMID: 27830514

60. Gajra B, Patel RR, Dalwadi C. Formulation, optimization and characterization of cationic polymeric nanoparticles of mast cell stabilizing agent using the Box–Behnken experimental design. Drug development and industrial pharmacy. 2016; 42(5):747–57. https://doi.org/10.3109/03639045.2015.1093496 PMID: 26559522

61. Morales-Cruz M, Flores-Fernández GM, Morales-Cruz M, Orellano EA, Rodriguez-Martinez JA, Ruiz M, et al. Two-step nanoprecipitation for the production of protein-loaded PLGA nanospheres. Results in pharma sciences. 2012; 2:79–85. https://doi.org/10.1016/j.rinphs.2012.11.001 PMID: 23316451

62. Lalani J, Patil S, Kolate A, Lalani R, Misra A. Protein-functionalized PLGA nanoparticles of lamotrigine for neuropathic pain management. AAPS pharmscitech. 2015; 16(2):413–27. https://doi.org/10.1208/s12249-014-0235-3 PMID: 25354788

63. Dizaj SM, Lotfipour F, Barzegar-Jalali M, Zarrintan M-H, Adibkia K. Box-Behnken experimental design for preparation and optimization of ciprofloxacin hydrochloride-loaded CaCO3 nanoparticles. Journal of drug delivery science and technology. 2015; 29:125–31.

64. Dora CP, Singh SK, Kumar S, Datusalia AK, Deep A. Development and characterization of nanoparticles of glibenclamide by solvent displacement method. Acta pol pharm. 2010; 67(3):283–90. PMID: 20524431

65. Devrim B, Kara A, Vural İ, Bozkır A. Lysozyme-loaded lipid-polymer hybrid nanoparticles: preparation, characterization and colloidal stability evaluation. Drug development and industrial pharmacy. 2016; 42(11):1865–76. https://doi.org/10.1080/03639045.2016.1180392 PMID: 27091346

66. Hallan SS, Kaur P, Kaur V, Mishra N, Vaidya B. Lipid polymer hybrid as emerging tool in nanocarriers for oral drug delivery. Artificial cells, nanomedicine, and biotechnology. 2016; 44(1):334–49. https://doi.org/10.3109/21691401.2014.951721 PMID: 25237838

67. Jung H, Ho M, Ahn S, Han Y, Kang M. Synthesis and physicochemical evaluation of entecavir-fatty acid conjugates in reducing food effect on intestinal absorption. Molecules. 2018; 23(4):731.

68. Salatin S, Barar J, Barzegar-Jalali M, Adibkia K, Kiafar F, Jelvehgari M. Development of a nanoprecipitation method for the entrapment of a very water soluble drug into Eudragit RL nanoparticles. Research in pharmaceutical sciences. 2017; 12(1):1. https://doi.org/10.4103/1735-5362.199041 PMID: 28255308

69. Massella D, Celasco E, Salaün F, Ferri A, Barresi A. Overcoming the limits of flash nanoprecipitation: Effective loading of hydrophilic drug into polymeric nanoparticles with controlled structure. Polymers. 2018; 10(10):1092.

70. Mandal B, Mittal NK, Balabathula P, Thoma LA, Wood GC. Development and in vitro evaluation of core–shell type lipid–polymer hybrid nanoparticles for the delivery of erlotinib in non-small cell lung

cancer. European journal of pharmaceutical sciences. 2016; 81:162–71. https://doi.org/10.1016/j.ejps.2015.10.021 PMID: 26517962

71. Duan R, Li C, Wang F, Yangi J-C. Polymer–lipid hybrid nanoparticles-based paclitaxel and etoposide combinations for the synergistic anticancer efficacy in osteosarcoma. Colloids and surfaces b: biointerfaces. 2017; 159:880–7. https://doi.org/10.1016/j.colsurfb.2017.08.042 PMID: 28892872

72. Hu Y, Hoerle R, Ehrich M, Zhang C. Engineering the lipid layer of lipid–PLGA hybrid nanoparticles for enhanced in vitro cellular uptake and improved stability. Acta biomaterialia. 2015; 28:149–59. https://doi.org/10.1016/j.actbio.2015.09.032 PMID: 26428192

73. Zhao P, Wang H, Yu M, Liao Z, Wang X, Zhang F, et al. Paclitaxel loaded folic acid targeted nanoparticles of mixed lipid-shell and polymer-core: in vitro and in vivo evaluation. European journal of pharmaceutics and biopharmaceutics. 2012; 81(2):248–56. https://doi.org/10.1016/j.ejpb.2012.03.004 PMID: 22446630

74. Wang AZ, Yuet K, Zhang L, Gu FX, Huynh-Le M, Radovic-Moreno AF, et al. ChemoRad nanoparticles: a novel multifunctional nanoparticle platform for targeted delivery of concurrent chemoradiation. Nanomedicine. 2010; 5(3):361–8. https://doi.org/10.2217/nnm.10.6 PMID: 20394530

75. Pagano R, Ruysschaert JM, Miller I. The molecular composition of some lipid bilayer membranes in aqueous solution. The journal of membrane biology. 1972; 10(1):11–30. https://doi.org/10.1007/bf01867845 PMID: 4656230

76. Shao XR, Wei XQ, Song X, Hao LY, Cai XX, Zhang ZR, et al. Independent effect of polymeric nanoparticle zeta potential/surface charge, on their cytotoxicity and affinity to cells. Cell proliferation. 2015; 48(4):465–74. https://doi.org/10.1111/cpr.12192 PMID: 26017818

77. Chen R, Wang S, Zhang J, Chen M, Wang Y. Aloe-emodin loaded solid lipid nanoparticles: formulation design and in vitro anti-cancer study. Drug delivery. 2015; 22(5):666–74. https://doi.org/10.3109/10717544.2014.882446 PMID: 24512431

78. Krishnamachari Y, Madan P, Lin S. Development of pH-and time-dependent oral microparticles to optimize budesonide delivery to ileum and colon. International journal of pharmaceutics. 2007; 338(1–2):238–47. https://doi.org/10.1016/j.ijpharm.2007.02.015 PMID: 17368982

79. Ali MH, Kirby DJ, Mohammed AR, Perrie Y. Solubilisation of drugs within liposomal bilayers: alternatives to cholesterol as a membrane stabilising agent. Journal of pharmacy and pharmacology. 2010; 62(11):1646–55. https://doi.org/10.1111/j.2042-7158.2010.01090.x PMID: 21039548

80. Hussain T, Saeed T, Mumtaz AM, Javaid Z, Abbas K, Awais A, et al. Effect of two hydrophobic polymers on the release of gliclazide from their matrix tablets. ACTA poloniae pharmaceutica-drug research. 2013; 70:749–57.

81. Zoubari G, Staufenbiel S, Volz P, Alexiev U, Bodmeier R. Effect of drug solubility and lipid carrier on drug release from lipid nanoparticles for dermal delivery. European journal of pharmaceutics and biopharmaceutics. 2017; 110:39–46. https://doi.org/10.1016/j.ejpb.2016.10.021 PMID: 27810471

82. Moran-Valero MI, Ruiz-Henestrosa VMP, Pilosof AM. Synergistic performance of lecithin and glycerol monostearate in oil/water emulsions. Colloids and surfaces b: biointerfaces. 2017; 151:68–75. https://doi.org/10.1016/j.colsurfb.2016.12.015 PMID: 27987457

83. Chen W, Palazzo A, Hennink WE, Kok RJ. Effect of particle size on drug loading and release kinetics of gefitinib-loaded PLGA microspheres. Molecular pharmaceutics. 2016; 14(2):459–67. https://doi.org/10.1021/acs.molpharmaceut.6b00896 PMID: 27973854

84. Win KY, Feng S-S. Effects of particle size and surface coating on cellular uptake of polymeric nanoparticles for oral delivery of anticancer drugs. Biomaterials. 2005; 26(15):2713–22. https://doi.org/10.1016/j.biomaterials.2004.07.050 PMID: 15585275

85. Aeschimann W, Staats S, Kammer S, Olieric N, Jeckelmann J-M, Fotiadis D, et al. Self-assembled α-tocopherol transfer protein nanoparticles promote vitamin E delivery across an endothelial barrier. Scientific reports. 2017; 7(1):4970. https://doi.org/10.1038/s41598-017-05148-9 PMID: 28694484

86. Rigotti A. Absorption, transport, and tissue delivery of vitamin E. Molecular aspects of medicine. 2007; 28(5–6):423–36. https://doi.org/10.1016/j.mam.2007.01.002 PMID: 17320165

87. Kulkarni SA, Feng S-S. Effects of particle size and surface modification on cellular uptake and biodistribution of polymeric nanoparticles for drug delivery. Pharmaceutical research. 2013; 30(10):2512–22. https://doi.org/10.1007/s11095-012-0958-3 PMID: 23314933

88. Bongiorno D, Ceraulo L, Ferrugia M, Filizzola F, Longo A, Mele A, et al. Interactions of α-tocopherol with biomembrane models: Binding to dry lecithin reversed micelles. International journal of pharmaceutics. 2006; 312(1–2):96–104. https://doi.org/10.1016/j.ijpharm.2006.01.017 PMID: 16481134

89. Mustafa S, Devi VK, Pai RS. Kanamycin sulphate loaded PLGA-vitamin-E-TPGS long circulating nanoparticles using combined coating of PEG and water-soluble chitosan. Journal of drug delivery. 2017; 2017.

90. Meng R, Li K, Chen Z, Shi C. Multilayer coating of tetrandrine-loaded PLGA nanoparticles: Effect of surface charges on cellular uptake rate and drug release profile. Journal of Huazhong university of science and technology [medical sciences]. 2016; 36(1):14–20. https://doi.org/10.1007/s11596-016-1535-5 PMID: 26838734

91. D'Addio SM, Bukari AA, Dawoud M, Bunjes H, Rinaldi C, Prud'homme RK. Determining drug release rates of hydrophobic compounds from nanocarriers. Philosophical transactions of the royal society a: mathematical, physical and engineering sciences. 2016; 374(2072):20150128.

92. Chan JM, Zhang L, Yuet KP, Liao G, Rhee J-W, Langer R, et al. PLGA–lecithin–PEG core–shell nanoparticles for controlled drug delivery. Biomaterials. 2009; 30(8):1627–34. https://doi.org/10.1016/j.biomaterials.2008.12.013 PMID: 19111339

93. Dobrovolskaia MA, Clogston JD, Neun BW, Hall JB, Patri AK, McNeil SE. Method for analysis of nanoparticle hemolytic properties in vitro. Nano letters. 2008; 8(8):2180–7. https://doi.org/10.1021/nl0805615 PMID: 18605701

94. Ishak RA, Mostafa NM, Kamel AO. Stealth lipid polymer hybrid nanoparticles loaded with rutin for effective brain delivery–comparative study with the gold standard (Tween 80): optimization, characterization and biodistribution. Drug delivery. 2017; 24(1):1874–90. https://doi.org/10.1080/10717544.2017.1410263 PMID: 29191047

95. Pooja D, Kulhari H, Singh MK, Mukherjee S, Rachamalla SS, Sistla R. Dendrimer–TPGS mixed micelles for enhanced solubility and cellular toxicity of taxanes. Colloids and surfaces b: biointerfaces. 2014; 121:461–8. https://doi.org/10.1016/j.colsurfb.2014.06.059 PMID: 25063311

96. Sengel-Turk CT, Hascicek C. Design of lipid-polymer hybrid nanoparticles for therapy of BPH: Part I. Formulation optimization using a design of experiment approach. Journal of drug delivery science and technology. 2017; 39:16–27.

97. Abdel-Bar HM, el Basset Sanad RA. Endocytic pathways of optimized resveratrol cubosomes capturing into human hepatoma cells. Biomedicine & pharmacotherapy. 2017; 93:561–9.